Rouvinski et al., http://www.jcb.org/cgi/content/full/jcb.201308028/DC1

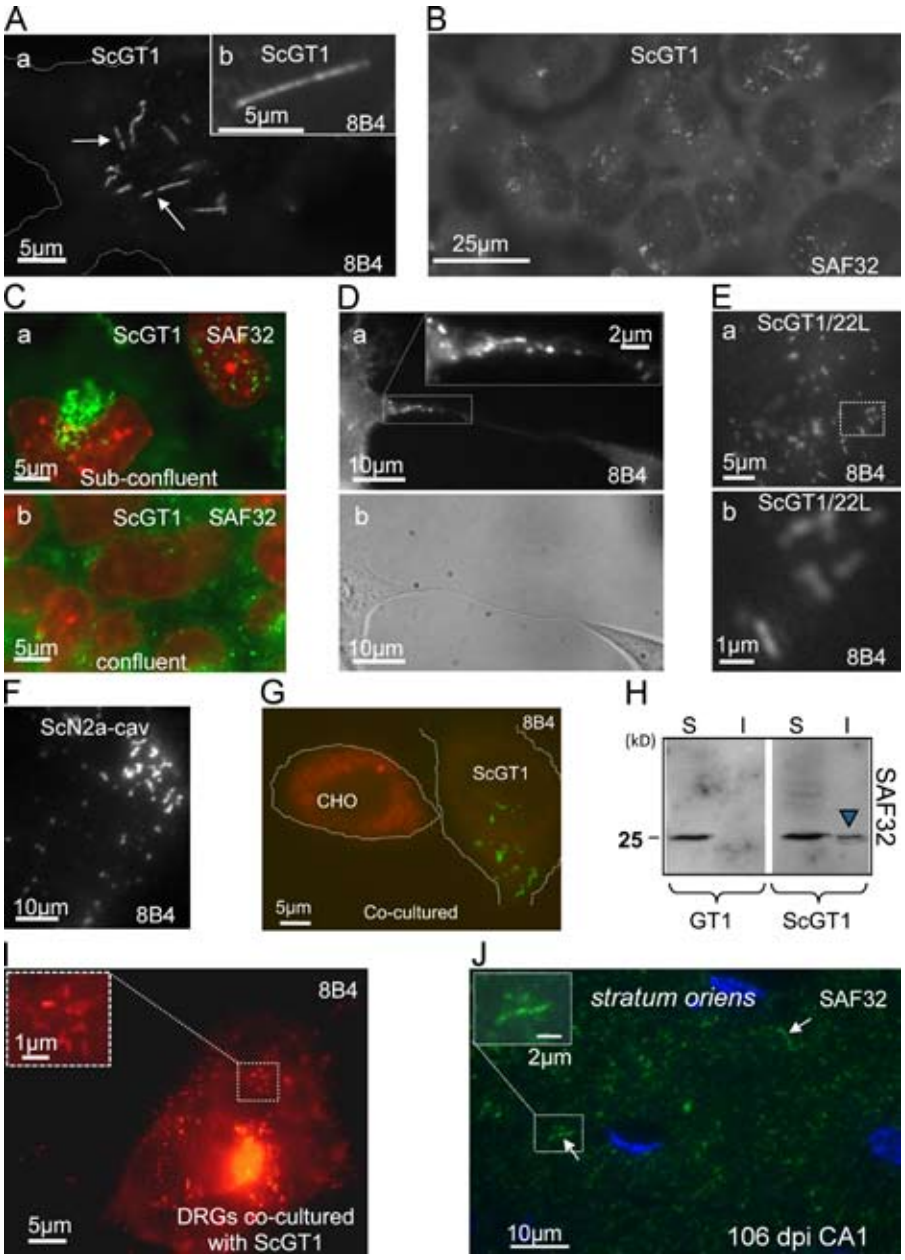

Figure S1. **N-proximal PrP Abs decorate clusters of micrometer-long strings specifically in prion-infected cells, primary mouse DRG cells, and brain.** (A–E) ScGT1 (A–C and E) and SMB (D) cells were fixed with formaldehyde, permeabilized, and stained with either mAbs 8B4 or SAF32, as indicated. (B–D) Cells were denatured with GdnSCN before staining. (A) Notice the interrupted (arrows) and sinuous strings. An exceptionally long string is shown in A (b). (B) Cells were photographed at low magnification to document the abundance of strings in every cell of the field. (C) Cells were counterstained with Hoechst (red) to visualize their degree of confluence. (C, a) Subconfluent cells contained abundant strings (green). When cells attain confluence, well-differentiated strings disappeared, perhaps replaced by small dots (b). (D) Strings on a connection between two SMB cells. (E) Strings in ScGT1 chronically infected with strain 22L. (F) ScN2a-cav cells growth arrested with distamycin A. (G) CHO cells were labeled with MitoTracker red, rinsed, and reseeded to co-culture with ScGT1 for 48 h. Cells were then cooled to 8°C, incubated with PIPLC, and stained with 8B4 followed by Cy2 secondary Fabs (as described for Fig. 4 A), and then visualized by fluorescence microscopy. Notice that CHO cells (which are not susceptible to prion infection) lack strings even when grown in proximity to a string-positive ScGT1 cell. (H) ScGT1 contain appreciable amounts of FL PrP^{Sc}. Lysates of uninfected GT1 and of infected ScGT1 cells were fractionated by sedimentation through sucrose-Sarkosyl gradients (as in Fig. 1 B). Fractions collected from the top (S: fractions 1–4) or the bottom (I: fractions 8–11) of the gradient were pooled, deglycosylated with PNGase F, and analyzed in WBs developed with N-terminal mAb SAF32. The arrowhead points to the deglycosylated highly aggregated FL PrP^{Sc} in ScGT1, which is absent from the corresponding I fraction of GT1 cells. (I) A cluster of mouse DRG cells in a dish of DRG co-cultured for 5 d with ScGT1 were fixed, permeabilized, and stained with 8B4. DRG cells were distinguished by the shape of the neuronal cell bodies from which bundles of straight, nontapering axons radiated. The DRG cell in the field has abundant strings. (J) SAF32 immunofluorescence (green) labeling of prion-infected hippocampus *stratum oriens* in a mouse 106 dpi. No epitope retrieval procedure was performed (compare with Fig. 1 E). Blue, DAPI; arrows, streaks of SAF32 immunofluorescence (enlarged in inset).

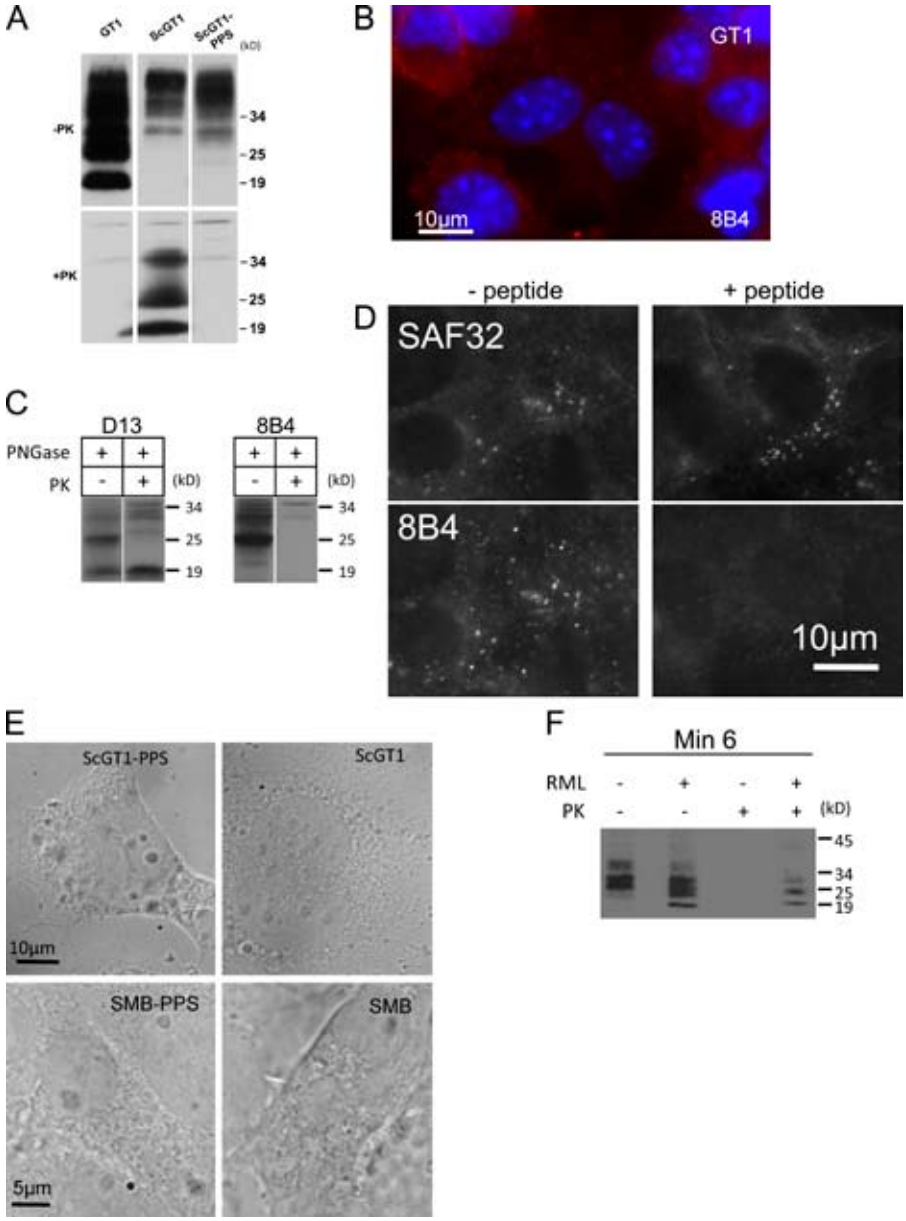

Figure S2. **Supporting data for Figs. 1 and 2.** (A) GT1 and cured ScGT1-PPS cells lack PrP^{Sc}. Cell lysates analyzed in WB developed with core Fab D13. In the bottom panel, lysates were digested with PK (20 µg/ml; 30 min at 37°C) before electrophoresis. (B) GT1 cells were labeled with 8B4 (red) as described for Fig. 1 C. No strings occur in these uninfected cells. Blue, DAPI. (C) 8B4 reacts with FL PrP^{Sc} but not PrP27-30. ScGT1 lysates, either untreated or treated with PK (+PK; 20 µg/ml; 30 min at 37°C), were deglycosylated with PNGase and analyzed in a WB developed either with core Fab D13 or with N-terminal mAb 8B4. 8B4 reacts with the 26-kD FL species but not with the 19-kD band, which comprises deglycosylated PrP27-30 molecules. (D) 8B4 reacts specifically with PrP in strings. SMB cells were fixed, denatured with FA, and colabeled with N-terminal mAbs 8B4 and SAF32. (right) The mAb mixture was preincubated with a peptide (8 µm/ml) mimicking the 8B4 epitope but unrelated to the SAF32 epitope. The peptide prevented the staining of strings by 8B4 but not by SAF32. (E) DIC images of the fields shown in Fig. 1 C (a, b, d, and e). (F) PK-resistant PrP in chronically infected Min6/RML. Cell lysates were analyzed in a WB developed with IPC1. Where indicated, lysates were digested with PK (20 µg/ml; 30 min at 37°C) before electrophoresis.

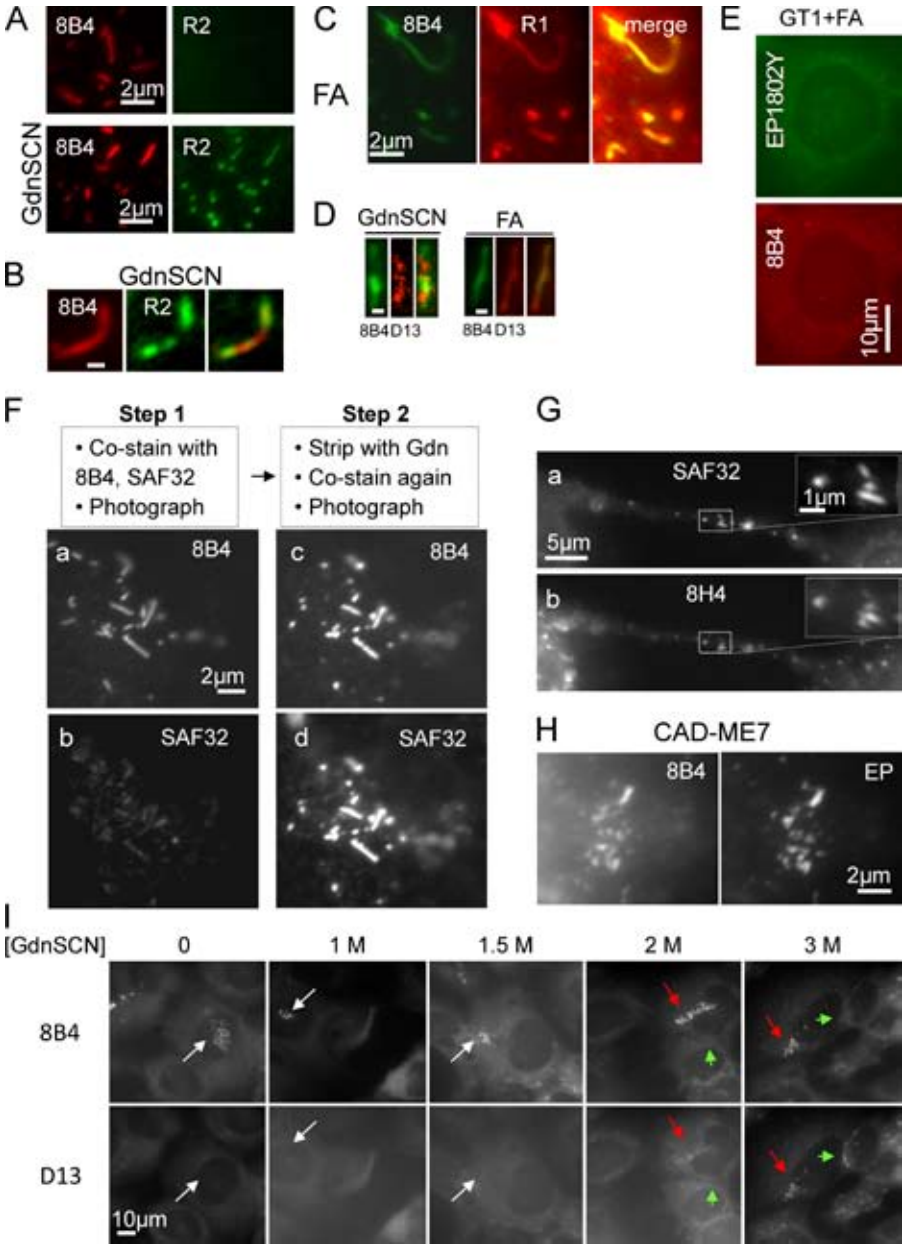

Figure S3. **Effects of FA and GdnSCN denaturation on string immunoreactivity.** GT1 (E) or ScGT1 (all other panels except H) cells were fixed with formaldehyde, permeabilized, denatured with FA or GdnSCN as indicated or left undenatured, and then immunostained with the indicated Abs. (A) The extreme C-terminal Fab R2 does not stain strings without prior denaturation, similar to all other core Abs tested in this study (summarized in Fig. 2 B). (B–D) Superior retrieval of PrP27-30 core epitopes by FA as compared with only intermittent exposure achieved by 3 M GdnSCN. (E) Denaturation does not induce strings in uninfected GT1 cells. Bars: (B and D) 0.5 μm. (F) Denaturation increases the staining of N-Abs but no new strings are revealed. (Step 1) Subconfluent ScGT1 growing on chambered coverslips were fixed, permeabilized, and costained with a mixture of mAbs 8B4 and SAF32 followed by subtype-specific secondary Abs (a and b), and then photographed. (Step 2) The cells were denatured with GdnSCN (3 M; 5 min), reblocked with BSA, and restained with the same primary and secondary Abs, and the same fields were rephotographed using strictly the same acquisition parameters (c and d). Strict controls confirmed that the denaturation completely stripped the primary Abs used in the first round of staining. 3 M GdnSCN increased the immunostaining intensity of 8B4 and SAF32 by ~2× and 6×, respectively. (G) PrP^{Sc} strings on intercellular connections revealed by denaturation staining protocol with both N- and core Abs. ScGT1 cells were costained with N-mAb SAF32 and core mAb 8H4 using the FA denaturing protocol and subtype-specific secondary Abs. (H) Strings in CAD cells infected with strain ME7. Fixed cells were denatured with FA before staining. (I) The D13 epitope is equally hidden in strings and in endosomal PrP27-30 stores. ScGT1 cells were fixed, treated with the indicated concentrations of GdnSCN (5 min at RT), and then costained with 8B4 and D13. Up to 1.5 M GdnSCN, D13 failed to decorate strings (white arrows) or endosomal stores. At 2 M, and more prominently at 3 M GdnSCN, D13 codecorated 8B4-positive strings (red arrows) and also revealed endosomal PrP27-30 stores (green arrows), which do not stain with N-terminal mAb 8B4.

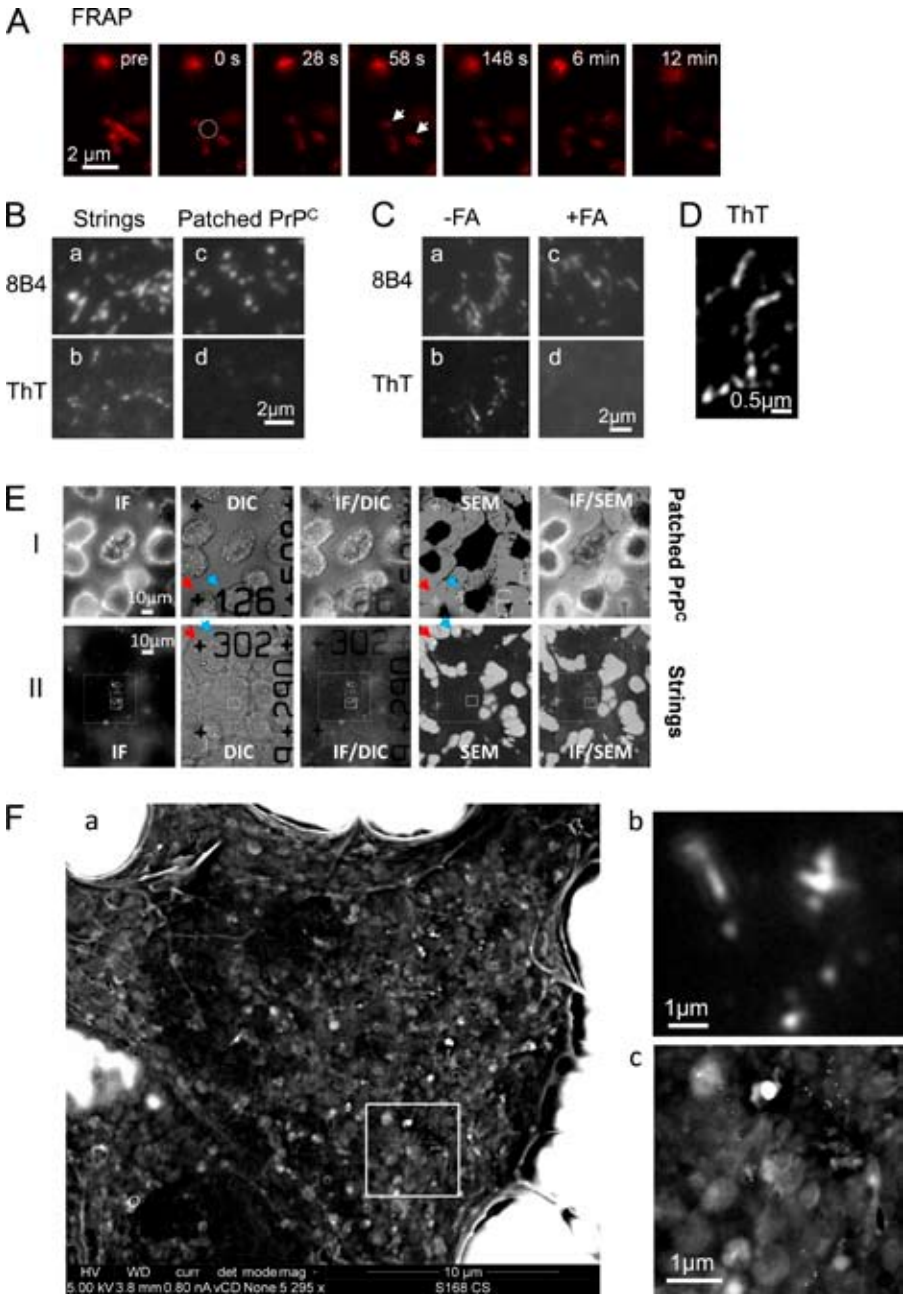

Figure S4. **Structural aspects of strings I.** (A) FRAP analysis of longitudinal diffusion along strings in live ScGT1 labeled with 8B4 followed by secondary Fab-RRX. There was no fluorescence recovery (arrows) in the photobleached area (indicated as a circle at 0 s). Furthermore, the remaining fluorescent ends of the string stayed associated in space throughout the observation period. (B and C) Specificity of ThT staining. (B) ScGT1 (a and b) and cured ScGT1-PPS (c and d) cells were labeled at 8°C with mAb 8B4, followed by a secondary Fab-RRX (ScGT1, Strings) or a polyclonal Ab-RRX to induce cell surface patching of PrP^C (ScGT1-PPS, Patched PrP^C). They were then subjected to a PM tear-off procedure, and the PM sheets adsorbed to coverslips were fixed with formaldehyde and stained with ThT. Even though PrP^C patches in the uninfected cells stained intensely with 8B4 (compare a and c), only the string structures in the infected cells fluoresced with ThT (compare b and d). (C) ScGT1 were labeled with 8B4 followed by a secondary Fab-RRX and then subjected to a tear-off procedure. The material transferred to the coverslips was fixed with formaldehyde and then stained with ThT. In c and d, fixed coverslips were incubated with 98% FA (2 min at RT) before staining with ThT. FA prevented string ThT fluorescence (compare d and b), whereas the 8B4-derived fluorescence remained after the FA treatment (a and c). (D) ThT staining was discontinuous and quasi-periodic along strings (2D deconvolution). (E and F) Correlative LM/SEM. Cells were grown on ITO-coated glass slides with a gold nanoruler visible by both DIC LM and SEM (E, arrows). Live ScGT1 cells (E [II] and F) were immunolabeled with 8B4 followed by secondary fluorescent and 18-nm immunogold labels (Materials and methods, Correlative LM/SEM). ScGT1-PPS (E and I) were labeled as above, except that a clustering Ab was used to induce PrP^C patches on the cell surface. In E [II] and in F, the ScGT1cells were treated with PIPLC before immunolabeling. In all panels, cells were fixed, visualized by immunofluorescence, postfixed, and further processed for SEM without metal coating. The nanoruler permitted positional correlation between LM and SEM. (E) each row represents a single field; LM (fluorescent and DIC) and SEM (BSe) images (low magnification); and overlays thereof are shown. (F) The ScGT1 field delineated by the dotted box in E was observed by higher magnification SEM (magnification of 5,295 in F [a] compared to 1,000 in E). Note that colloidal gold was readily visible using BSe even at this relatively low magnification (inset in a, magnified in c) and correlated well with strings seen by immunofluorescence (compare b and c). A higher magnification image of the field in c is shown in Fig. 6 E (a). The length of the immunogold bridge limits the lateral resolution to ~40 nm (Materials and methods, Correlative LM/SEM).

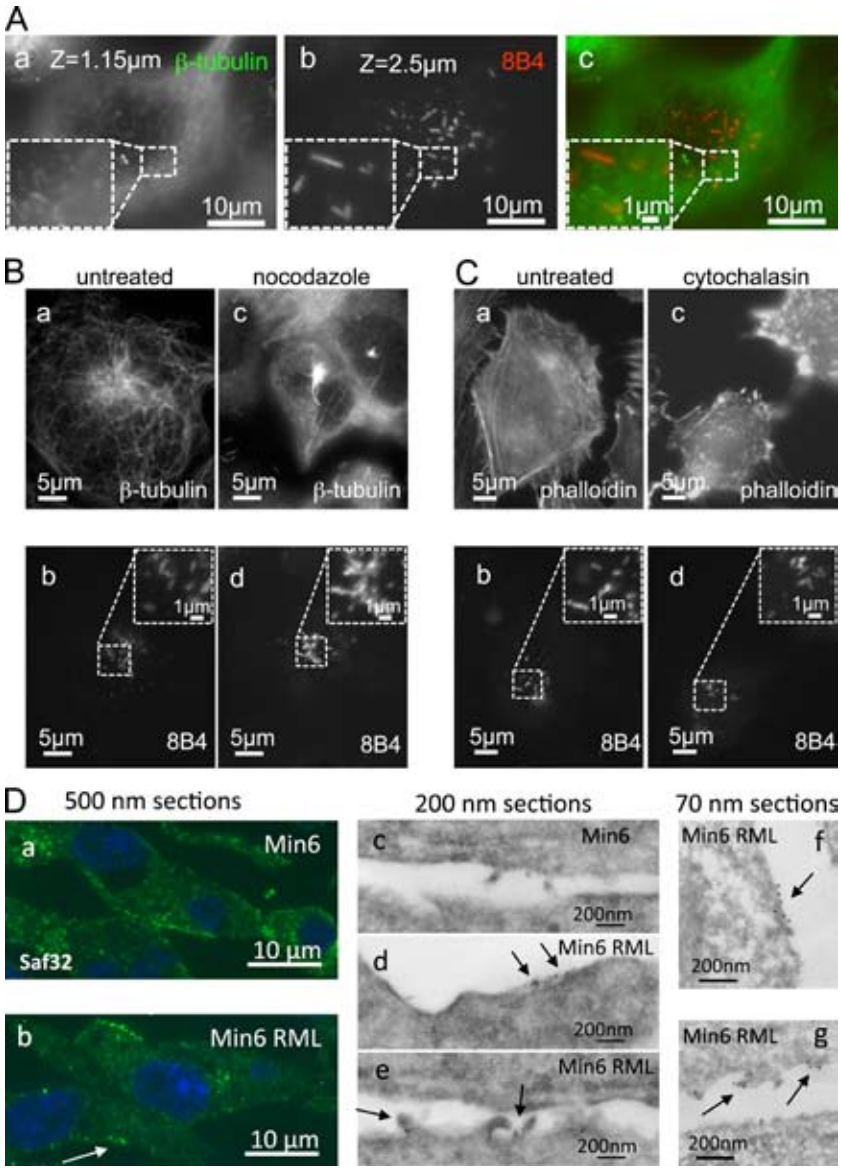

Figure S5. **Structural aspects of strings II.** (A–C) Strings do not coincide with microtubules; strings withstand short-term cytoskeleton disruption with nocodazole or cytochalasin D. (A) Fixed and permeabilized ScGT1 cells were stained with mAb 8B4 (b; red in the merged micrographs in c) and costained with a β-tubulin Ab (a; green in c). Microscopic z-stacks were acquired, and 8B4 and cytoskeletal staining were compared in several focal planes. We found no colocalization or alignment between the strings and the cytoskeletal elements. We also failed to discern higher scale organizations in fibers that would correspond to string clusters. Note that the tubulin and PrP panels in A represent two focal planes 1.35 µm apart, as strings are located more peripherally than the microtubule web. (B and C) ScGT1 cells were treated with either nocodazole (0.1 µM; 30 min; B) or cytochalasin D (2 µM; 15 min; C) to inhibit the tubulin or actin cytoskeletons, respectively. They were then fixed with MeOH at −20°C (B) or fixed with formaldehyde (37°C for 45 min) and then permeabilized with Triton X-100 (C). Cells were then stained with 8B4 and costained with a β-tubulin Ab (B) or with phalloidin-rhodamine (C) to show microtubules and f-actin, respectively. Disrupting these cytoskeletal elements (compare a and c) did not alter the shape of the strings (compare b and d, respectively), suggesting that strings were not directly specified by these fibers. (D) TEM. Min6 and Min6 RML cells were fixed, scraped off the dish, pelleted, cryosectioned, and immunolabeled with SAF32 followed either by secondary fluorescent Ab (a and b) or with a bridging Ab followed by protein A–10-nm gold (Materials and methods). (D, a and b) Threads of PrP foci in 500-nm sections of infected Min6/RML cells (b, arrow), but not in uninfected controls (a). (d and e) 200-nm sections are shown of infected cells with gold clusters (arrows) on the plasma membrane. (e) The clusters are associated with membrane structures reminiscent of macropinocytic processes. There was no gold in uninfected cells (c). (f and g) Clusters of immunogold in thin 70-nm sections through infected cells. Clusters may correspond to 100–200 nm PrP^{Sc} foci (see Fig. 10 B, Model B). In f, no structural feature is evident on either side of the PM in association with the clusters. In g, clusters are localized at membrane protrusions (similar to e).

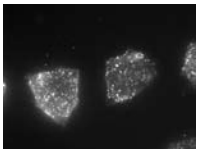

Video 1. **FL PrP^C dots are mobile on the surface of live GT1 cells.** (Related to Fig. 5 B, a.) Cells were labeled at 8°C with 8B4 and fluorescent secondary Fabs, warmed gradually to 24°C, and analyzed by time-lapse wide field fluorescence microscopy (Axiovert 200M; Carl Zeiss; using an NA 1.3, 100× Plan Neofluar objective) at 400 ms/frame. Time of movie, 24 s; length, 60 frames. Many small dots (with integrated intensity of ∼0.3 arbitrary units; Fig. 5 C, b) move rapidly (mean mobility of 0.4 µm/s; Fig. 5 C, a).

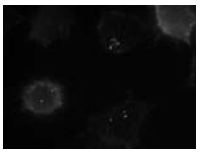

Video 2. **Clusters of Ab-patched FL PrP^C are largely immobile on the surface of live GT1.** (Related to Fig. 5 B, b.) Cells were labeled at 8°C with 8B4 followed by fluorescent secondary Fabs and by tertiary polyvalent clustering Ab. Cells were then warmed gradually to 24°C and analyzed by time-lapse wide field fluorescence microscopy (Axiovert 200M; Carl Zeiss; using an NA 1.3, 100× Plan Neofluar objective) at 400 ms/frame. Time of movie, 24 s, length, 60 frames. Large, intensely staining patches of FL PrP^C (with integrated intensity of ∼5 arbitrary units; Fig. 5 C, b) are relatively immobile (mean mobility 0.03 µm/s; Fig. 5 C, a). Notice that many surrounding small 8B4 dots of lower intensity are still very mobile.

Video 3. **PrP^{Sc} strings on the surface of live ScGT1 cells are immobile, akin to clusters of patched PrP^C.** (Related to Fig. 5 B, c.) Cells were labeled at 8°C with 8B4 followed by fluorescent secondary Fabs. Cells were then warmed gradually to 24°C and analyzed by time-lapse wide field fluorescence microscopy (Axiovert 200M; Carl Zeiss; using an NA 1.3, 100× Plan Neofluar objective) at 400 ms/frame. Time of movie, 24 s; length, 60 frames. Strings of FL PrP^{Sc} are as immobile as are the clusters of PrP^C in uninfected cells (compare with Video 2; mean mobility 0.03 µm/s; Fig. 5 C, a). Note the many small, very mobile 8B4 dots of lower intensity. These dots are removed by treating cells PIPLC (Video 4).

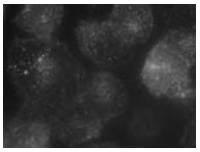

Video 4. **Slow moving PrP^{Sc} strings and dots on the surface of live ScGT1 cells represent a major pool of surface PIPLC-resistant FL PrP^{Sc}.** (Compare with Video 3.) Cells were cooled to 8°C, digested with PIPLC, and labeled with 8B4 followed by fluorescent secondary Fabs. Cells were then warmed gradually to 24°C and analyzed by time-lapse wide-field fluorescence microscopy (Axiovert 200M; Carl Zeiss; using an NA 1.3, 100× Plan Neofluar objective) at 400 ms/frame. Time of movie, 24 s; length, 60 frames. Strings and their associated dots of FL PrP^{Sc} are slow moving objects representing a major part of surface PIPLC-resistant FL PrP^{Sc}.

Table S1. **Subcellular markers and endocytic tracers which do not co-localize with strings**

Category	No.	Marker	Organelle/structure
Internalized tracers	1	Internalized dextran[a]	Late endocytic organelles (when fed to cells continuously for >2 h)
	2	Internalized fluorescent aerolysin[a]	Recycling and/or late endosomes (Fivaz et al., 2002)
Intracellular markers	3	Rab 4A, 5A, and EEA1	Early endosomes
	4	Rab 7 and 9	Late endosomes
	5	Rab 11	Recycling endosomes
	6	BiP and Calnexin	ER
	7	M6PR	TGN and lysosomes
	8	LAMP1; lysoTracker[a]	Late endosomes/lysosomes
	9	GM130	Golgi
	10	Clathrin	Clathrin-coated pits and TGN
	11	BODIPY[a]	Lipid droplets
	12	Flotillin 1 and 2	Raft-related vesicles (Pimpinelli et al., 2005; Stuermer et al., 2004)
	13	Pacsin 2 (EHD2)	Membrane tubules (Hansen et al., 2011)
Cytoskeletal markers	14	Tubulin	Microtubules
		f-actin (phalloidin)	Microfilaments

In all experiments except No. 1, cells were fixed before microscopic examination. Internalized dextran in No. 1 was observed both in fixed and in live cells, to allow the detection of temperature- and/or fixation-sensitive endocytic structures such as the GPI-AP–enriched endosomal compartment involved in GPI-AP endocytosis (Sabharanjak et al., 2002).
[a]Live cells were incubated with the reagents before fixation.

References

Fivaz, M., F. Vilbois, S. Thurnheer, C. Pasquali, L. Abrami, P.E. Bickel, R.G. Parton, and F.G. van der Goot. 2002. Differential sorting and fate of endocytosed GPI-anchored proteins. *EMBO J.* 21:3989–4000. http://dx.doi.org/10.1093/emboj/cdf398

Hansen, C.G., G. Howard, and B.J. Nichols. 2011. Pacsin 2 is recruited to caveolae and functions in caveolar biogenesis. *J. Cell Sci.* 124:2777–2785. http://dx.doi.org/10.1242/jcs.084319

Pimpinelli, F., S. Lehmann, and I. Maridonneau-Parini. 2005. The scrapie prion protein is present in flotillin-1-positive vesicles in central- but not peripheral-derived neuronal cell lines. *Eur. J. Neurosci.* 21:2063–2072. http://dx.doi.org/10.1111/j.1460-9568.2005.04049.x

Sabharanjak, S., P. Sharma, R.G. Parton, and S. Mayor. 2002. GPI-anchored proteins are delivered to recycling endosomes via a distinct cdc42-regulated, clathrin-independent pinocytic pathway. *Dev. Cell.* 2:411–423. http://dx.doi.org/10.1016/S1534-5807(02)00145-4

Stuermer, C.A., M.F. Langhorst, M.F. Wiechers, D.F. Legler, S.H. Von Hanwehr, A.H. Guse, and H. Plattner. 2004. PrPc capping in T cells promotes its association with the lipid raft proteins reggie-1 and reggie-2 and leads to signal transduction. *FASEB J.* 18:1731–1733.